Inkjet Printing of Latex-Based High-Energy Microcapacitors

Fernando Torres-Canas, Jinkai Yuan, Isabelle Ly, Wilfrid A Neri, Annie Colin, Philippe Poulin

Inkjet Printing of Latex Based High-Energy Microcapacitors

Fernando Torres-Canas, Jinkai Yuan, Isabelle Ly, Wilfrid Neri, Annie Colin, and Philippe Poulin**

Dr. F. Torres-Canas, Dr. J. Yuan, I. Ly, W. Neri, Prof. A. Colin, Dr. P. Poulin
Univ. Bordeaux
CNRS, Centre de Recherche Paul Pascal, UMR5031
33600 Pessac, France
E-mail: jinkai.yuan@crpp.cnrs.fr, philippe.poulin@crpp.cnrs.fr

Keywords: inkjet printing, micro-energy storage device, PVDF latex, discharged energy density, dielectrics, polymer composites

Micro-energy storage devices are appealing, and highly demanded for diverse miniaturized electronic devices, ranging from microelectromechanical system, robotics, to sensing microsystems and wearable electronics. However, making high-energy microcapacitors with currently available printing technologies remains challenging. Herein, we show the possibility to use latex polyvinylidene fluoride (PVDF) as aqueous ink for making dielectric capacitors on the microscale. The dielectric properties of printed microcapacitors can be optimized based on a novel approach, i.e., mixing PVDF latex with polyvinyl alcohol (PVA) to realize dielectric organic nanocomposites. The PVA prevents the coalescence of PVDF nanoparticles and serves as a continuous matrix phase with high dielectric breakdown strength. While the well-dispersed PVDF nanoparticles serve as highly polarizable and isolated domains, providing large electric displacement under high fields. Consequently, a high discharged energy density of 12 Jcm^{-3} is achieved at 550 MVm^{-1}. These printed microcapacitors demonstrate mechanical robustness and dielectric stability over time.

1. Introduction

The rapid development of printed and flexible electronics with miniaturization and smart functionalities has accelerated the innovation of printed energy storage components.[1,2] The emerging micro-energy storage devices provide excellent micro-scale peak power. They can be easily integrated into other miniaturized electronic devices, such as energy-harvesting microelectromechanical system, microrobotics, sensing microsystems, biomedical implants, portable and wearable personal electronics.[3,4] Micro-batteries and micro-supercapacitors represent newly developed miniaturized electrochemical energy storage devices. They have high gravimetric energy density but fall short of the rising demands of rapid charging/discharging, high cycling and charge retention for the next-generation of micro-energy storage devices. Electrostatic capacitors are the only energy storage methodology with intrinsically high power densities (on the order of Megawatt per kg).[5] They are appealing for reliable and efficient electric microsystems. However, the printed dielectric capacitors have a low energy density that is approximately three orders of magnitude less than printable microsupercapacitors.[4,5] Today, this drawback leads to large printing area and high system weight. Therefore, developing new printable microcapacitors with improved energy density is imperative to enable the reduction of size, weight, and cost of the modern printing power electronics. The discharged energy density (U_e) of a dielectric capacitor is expressed by

$$U_e = \int_{D_{max}}^{0} EdD \quad (1)$$

where E is the applied electric field, and D is the electric displacement. The key to improve the energy density of dielectric materials is to achieve a high breakdown strength (E_b) associated to a large electric displacement D_{max}.

To date, dielectric microcapacitors are mainly fabricated by spin coating, dip coating, lithography, and inkjet printing.[6–11] Inkjet printing is considered as particularly promising

because of its easy scalability. Also, it allows for a good control of the micrometric patterns on-demand. So far, most of the inkjet-printed capacitors have been realized by depositing droplets of ceramic nanopowder suspensions and/or polymer dielectric inks.[12–18] In particular, films of high-*k* metal oxides, such as $BaTiO_3$, IZO, HfO_2, have been printed. However, these films are brittle and need post treatments at high annealing temperatures. As alternatives, polymeric materials, such as SU-8 resin and poly(4-vinylphenol) (PVP), are more appealing due to their low-temperature processing, high breakdown strengths, low losses, and high reliability.[18–20] However, the low dipole moments of the chemical bonds in these polymers lead to low dielectric constants (k<4), giving rising to a low energy density (<3 Jcm^{-3}).[20,21] By contrast, polar polymers, such as polyvinylidene fluoride (PVDF)-based ferroelectric polymers are particularly promising for energy storage due to the unique combination of high dielectric constant and high breakdown strength.[21–23] Haque et *al.* developed inkjet printing of films by starting from organic inks of high-molecular-weight polyvinylidene fluoride-trifluoroethylene P(VDF-TrFE) and investigated the morphology and crystallinity of the printed films.[24] Unfortunately, no dielectric properties were reported. More recently, Thuau et *al.* have made a progress by integrating P(VDF-TrFE) layers into inkjet-printed flexible electronic devices.[25] This polymer has a high cost, and is processed in harmful organic solvents, but it can be useful to make efficient sensors and actuators.[25] However, the dielectric properties of printed lower-cost PVDF materials are seldom reported, and inkjet-printed PVDF-based microcapacitors with superior energy storage performances have not been realized yet.

Herein, we report a high-energy flexible microcapacitor fully inkjet-printed on a poly(ethylene naphthalate) (PEN) substrate. The devices are made from water-based inks, a mixture of PVDF latex particles and polyvinyl alcohol (PVA). The rationale behind lies in the combination of the high polarization of PVDF and high breakdown strength of PVA for achieving high discharged energy density at high electric field. The mixture is printed as

dielectric layers sandwiched between two carbon nanotube (CNT) electrodes. These electrodes are also deposited by inkjet printing water-based CNT inks. The capacitance of printed microcapacitors can be tuned through the thickness of printed dielectric layers. The thickness is changed via controlling the inkjet printing parameters such as ink drop spacing, and number of printing passages. The obtained microcapacitors show high flexibility and stable capacitance even under large bending deformation. In addition, the microcapacitor displays a discharged energy density U_e, as high as 12 Jcm^{-3} at 550 MVm^{-1}. This remarkable value represents an improvement of 400 % as compared to films formulated with single PVDF or single PVA components. The environmentally friendly water based inks coupled with the superior energy storage performances of printed dielectrics makes our microcapacitors promising for demanding printed electronics that require micro-scale peak powers.

2. Results and Discussion

2.1 Inkjet printing of microcapacitors

As schematically demonstrated in **Figure 1a-c**, three steps were involved to print a microcapacitor. First, a multi-walled carbon nanotubes (MWNTs) aqueous ink was used to print a 30-mm-long and 140-μm-wide electrode layer on PEN substrate. Afterwards, 5 layers with a length of 20 mm were consecutively printed using the mixture of PVDF-PVA as dielectric ink on the surface of the electrode, leaving 10 mm electrode uncovered for the contact of following dielectric characterizations. At the end, an upper 30 mm long electrode was printed again on the top of the PVDF-PVA layer to formulate a sandwiched structure (**Figure 1d**), making sure that two electrode layers are in parallel but do not contact with each other. The entirely printed microcapacitor has an effective opposing electrode area of 20 mm × 140 μm, and enjoys high flexibility (**Figure 1e)**.

Generally, with a given viscosity of ink materials, the thickness of printed layer is determined by the spacing between two consecutive droplets (d_s) and the number (n) of the printing passages. Here, both of the bottom and top CNT electrodes are single passage layers with a width of 140 μm and a conductivity above 2100 Sm^{-1}. **Figure 2a** shows the microscopic image of the bottom electrode which is straight and uniform, evidenced by the 3D image of the thickness profile as well (**Figure 2d**). The average value of electrode thickness was measured at about 280 nm (**Figure 2e**). The printed PVDF-PVA layers fully cover the bottom electrode and well separate it from the upper one to formulate a parallel plate microcapacitor configuration (**Figure 2b-c**). The sectional SEM image of the entirely printed structure is shown in **Figure 2f**. The capacitance was tailored by varying the thickness of PVDF-PVA dielectric layer via controlling the inkjet printing parameters d_s and n.

It is well known that the capacitive performance and energy storage density of a microcapacitor largely relies on the quality of the dielectric films. A uniform and defect-free dielectric layer is the key for a printed microcapacitor to sustain high electric field. We first tried to print PVDF layers with pure latex (44 wt.%) and evaporate the water at low temperatures (<40 °C). The dried PVDF film is full of microcracks and easily detached from the PEN substrate (**Figure 3**). This phenomenon is similarly observed in soil science and other drying processes of colloids.[26–28] In general, when a wet thin film containing suspended colloidal nanoparticles is dried on a substrate, the evaporation of the solvent concentrates the nanoparticles into a closed packed arrays[29] with strong capillary forces acting on the film.[30] The latter generally binds to the substrate and resists deformation in the transverse direction giving rise to transverse tensile stresses.[31] In the case of soft particles, they deform to close the pores, but for hard particles, the film cracks to release the stresses. Different strategies have been proposed in recent years to reduce crack formation. Variations in particle size, shear modulus, interparticle forces, and thermodynamic properties (temperature, humidity, or gas flow rate), have all been shown to affect the shape and appearance of cracks.[32] In our

case, we first kept the PVDF latex ink composition unchanged and optimized the temperature of the printer plate (T_s). With increasing the temperature T_s up to 70 °C, the number of cracks is largely decreased, as shown in the upper images of **Figure 3**. Unfortunately, we were not able to reduce all cracks by solely optimizing the thermal conditions. Such cracks bring the risk of short cuts between two printed CNT electrodes and eventually the failure of microcapacitors. Even spin-coated PVDF latex film presents also voids on the micrometer scale (**Figure S1a**). However, the addition of PVA (7wt.% of PVA) is shown to not only increase the breakdown strength, but also to act as plasticizer allowing homogeneous film (**Figure S1b**). Compared to the pure PVDF latex, the evaporation of PVDF-PVA composite ink at low temperatures (<40 °C) leads to much less cracks, as shown in the bottom images of **Figure 3**. Interestingly, as the temperature of the plate T_s further increases, less and less cracks appear until a defect-free PVDF-PVA layer is achieved at T_s=70°C. Such conditions were kept for all printed microcapacitors in this research.

2.2 Capacitive behavior of the printed microcapacitors

The capacitive behavior of the printed microcapacitors is characterized by impedance spectroscopy. **Figure 4a** shows the area/thickness (A/t) ratio dependent capacitance (black points, measured at 100 Hz) that can be tuned by varying d_s and n. The maximum drop spacing that allows for printing a continuous and homogeneous film was observed at 100 µm, giving a thinnest (5 µm) single polymer layer and thus the highest capacitance of about 38 pF with the capacitor geometry presented in **Figure 1**. Herein, the electrode area A is fixed. As increasing the thickness by the decline in d_s or the increase in n (inset of **Figure 4b**), the capacitance decreases linearly with reducing the values of A/t ratio. The slope represents the dielectric constant of the printed materials. A comparison is performed between our latex based microcapacitors and the previously reported ones based on polymers or ceramics (**Figure 4a**).[17,33,34] It is found that at the same printing A/t ratio, the PVDF based microcapacitors exhibit higher capacitance than hexagonal boron nitride (hBN) and polyimide

(PI)-based capacitors, but lower than the ones based on HfO_2. This is consistent with the order in terms of the value of dielectric constant for different printed materials. The dielectric constant can be determined by the following relationship[35]

$$C = \varepsilon_r \varepsilon_0 \frac{A}{t} \quad (2)$$

where C is the capacitance, ε_r is the relative dielectric constant and ε_0 is the permittivity of free space. **Figure 4b** presents the dielectric constant as a function of printing layer number at different d_s. The values remain constant around ~10 at 100 Hz for all the microcapacitors. It should be noted that this value is close to the ε_r already reported in the literature for PVDF films casted from polymer-organic solvent solutions.[36] This indicates that the introduction of a small amount of PVA does not affect the polarization behavior of the PVDF polymer. Meanwhile, the dielectric losses of all PVDF polymer still stay at a low level ($tan\delta$~0.06 at 100 Hz). The frequency dependences of the dielectric constant, conductivity, and loss tangent are presented in **Figure S2**.

Bending test allows the performance of the electrodes and of the microcapacitor under mechanical deformation to be studied (with a maximum amplitude of 10 mm (**Figure 5a**). It can be clearly seen in **Figure 5b-c** that the conductivity of the electrodes, and the capacitance of the microcapacitor, remained unchanged after bending cycles.

2.3 Energy storage properties of printed microcapacitors

In addition to the high polarizability, the dielectric breakdown strength, which has a quadratic effect on the charge storage capacity, is another critical metric of dielectric materials. The failure probability of printed PVDF-PVA dielectric layers was measured, and analyzed according to the Weibull distribution function, which is described as follows[37]

$$P(E) = 1 - e^{-(E/E_b)^{\beta}} \quad (3)$$

where $P(E)$ is the cumulative failure probability, E is the measured breakdown strength, E_b is the Weibull breakdown strength with 63.2 % probability to breakdown, and β the so-called

shape parameter which evaluates the scatter of the data. The characteristic dielectric breakdown strength is then extracted from the fitting based on the Weibull failure distribution function. As shown in **Figure 6a**, E_b for single layer of PVDF-PVA is 194 MVm^{-1}. E_b increases with the layer number and reaches 571 MVm^{-1} for 4 layers of PVDF-PVA. It should be noted that the breakdown strength of the 4-layers PVDF-PVA system is far higher than that of PVDF latex films (167 MVm^{-1}). It actually remains comparable to the pure PVA film (541 MVm^{-1}) (**Figure S3**). Concurrently, the β value increases from 3.26 for 1 printed layer to 8.57 for 4 printed layers, suggesting a narrow distribution of the breakdown strength of the 4 printed layers, indicative of improved dielectric reliability. **Figure 6b** shows the *P-E* loops of the microcapacitor (d_s=75 µm, and 4 PVDF-PVA layers) at different applied electric fields. It is found that the PVDF-PVA enjoys high polarization a maximum charge density of 55 mCm^{-2} at 550 MVm^{-1}. Such charge density is higher than that of pure PVA (28 mCm^{-2} at 600 MVm^{-1}, **Figure S4a**) or pure PVDF (20 mCm^{-2} at 260 MVm^{-1}, **Figure S5a**). Hysteresis leads to reduced efficiency, internal heating and ultimately limits the maximum energy density and the operational frequency of the capacitor.[38] In the present case, the hysteresis of the *P-E* loop increases very slowly with the applied electric field as compared to the PVA films (**Figure S4a**).

The discharged energy density (calculated according to the **Equation 1**), is derived from the *P-E* loops.[22,39] **Figure 6c** shows the discharged energy density as a function of the applied electric field for microcapacitors printed from 1 to 4 layers. Clearly, all discharged energy densities increase with increasing the electric field up to 300, 400, 670 and 550 MVm^{-1} for 1, 2, 3 and 4 printed layers, respectively. Nevertheless, the most striking feature is that the microcapacitor printed with 4 layers exhibits a large discharged energy density of ~12 Jcm^{-3}. This energy density rivals or exceeds the pristine PVDF materials already reported in the literature.[36,40,41] It is also six times higher than pure PVDF latex printed with the same 4

layers (**Figure S5b**) and one order of magnitude higher than the commercial BOPP capacitor (2 Jcm^{-3}).[21]

For practical applications of dielectric capacitors, it is important not only to have a high energy density, but also to maintain a high charge-discharge efficiency (η). The efficiency η is defined as:

$$\eta = \frac{U_d}{U_s} = 1 - \frac{U_l}{U_s} \quad (3)$$

where U_s, U_d and U_l are the stored, discharged energy and energy loss, respectively.[39] U_l is calculated by the numerical integration of the closed area of the hysteresis *P-E* loops. The efficiency of the microcapacitor decreases with the applied electric field, because of conduction losses.[42] It is clearly shown that the efficiency is presently enhanced with the number of printed layers, i.e., it goes from 0.3 at 300 MVm^{-1} for 1 printed layer to 0.74 at 550 MVm^{-1} for 4 printed layers (**Figure 6d)**. For comparison, the PVA and PVDF latex have a similar discharged energy density (~2.2 Jcm^{-3}, **Figure S4b** and **S5b**) however, the efficiency is around 0.78 for PVDF (**Figure S5c**) with respect to 0.3 for PVA (**Figure S4c**).

For dielectric materials, it is desirable to simultaneously achieve high discharged energy density and high efficiency. **Figure 7** compares the energy storage performances of the present inkjet printed PVDF-PVA nanocomposites and other polymer films prepared with conventional techniques such as solution casing or melt-extrusion.[43–54] All references data are reported near the breakdown strength. It is noted that most of the dielectric materials that enjoy an efficiency greater than 75% exhibit energy density U_e below ~10 Jcm^{-3}. Particularly, BOPP delivers the best efficiency (96 %), but its U_e is only 2 Jcm^{-3}. Comparatively, PVDF and its copolymers can achieve a U_e beyond ~10 Jcm^{-3} but their efficiency falls below 60%. By contrast, our microcapacitor possesses the overall U_e performance with a value of ~12 Jcm^{-3} and an efficiency of 74 %.

2.4 Morphologies of the printed PVDF-PVA dielectric layer

In order to clarify the properties of the present capacitors, we carried out scanning electron microscopy on the surface of printed dielectric layers. Two effects are observed: *i*) for 1 and 2 printed layers (**Figure 8a, b**) the PVDF-PVA still shows some cracks in spite of the process optimization described earlier. It is well known that the breakdown strength is strongly influenced by interface area, agglomeration and/or voids in the polymer composites.[38,55,56] These factors result in inhomogeneous electric field and in the decrease of the effective breakdown strength in the polymer composites. *ii*) for 3 and 4 printed layers (**Figure 8c-d**) no cracks were observed, resulting in a high discharged energy density. The added PVA to the PVDF latex prevents the coalescence of the PVDF, causing a homogeneous distribution of the PVDF nanoparticles (**Figure 8)**. It also acts as an efficient barrier to limit the formation of a degraded conducting path throughout PVDF nanoparticles. As a consequence, the present material can uniquely combine the high breakdown strength of PVA and the high permittivity of PVDF. The use of water based inks offers the possibility to easily use additives in the systems. This is demonstrated, for example, with the addition of high-*k* $BaTiO_3$ (BTO) nanoparticles to the system PVDF-PVA in order to improve the discharged energy density via increasing the permittivity (Figure S6 and S7).[39]

3. Conclusion

We used a low-cost and environmentally friendly water-based PVDF latex to achieve high-energy and high-efficiency miniaturized capacitor with inkjet printing technology. The achieved performances are much higher than that of pure PVDF latex, and PVA. The PVA not only allows a homogeneous film to be obtained, but also improves the breakdown strength of the polymer mixture. The obtained systems are compact polymer with few defects, which results in a higher discharged energy density and high efficiency. We also put in evidence the superior mechanical robustness and dielectric stability of the microcapacitors over time.

4. Experimental Section

MWNTs water-ink: Multi-walled carbon nanotubes (10-15 nm in diameter) were supplied by ARKEMA without any modification and were used as received. Bile salts (BS) were used as a surfactant to stabilize the nanotubes in water. The dispersion of MWNTs was prepared at 1 wt.% using a ratio of 1:1 between MWNTs and BS. The sonication process was performed using a 3 mm microtip for 30' with 1sec on/off pulses. The dispersion was placed in an ice bath to avoid overheating. Centrifugation (30' at 2200g) was performed in order to remove large aggregates and not dispersed MWNTs. Finally, the suspension was mixed with 10% of ethylene glycol (EG) to prevent the coffee ring formation and obtain homogeneous electrodes.

PVDF latex solution: The solution was supplied by ARKEMA (Kynar Aquatec® ARC Latex) with an initial concentration of solid content of 44 wt.%, and then diluted with deionized water down to 16 wt.% before being used as aqueous ink under the label of PVDF latex. An additional mixture of the original PVDF latex was prepared with a 2 wt.% solution of PVA (86000 g/mol) at a ratio of 93/7 between PVDF and PVA. This ink was labeled as PVDF-PVA. In this work, the PVDF/PVA mass ratio (93/7) was achieved by evaluating both the homogeneity of the film and the breakdown strength of PVDF-PVA composite with respect to PVA film. The ratio of 93/7 allows for crack-free films with high breakdown strength.

Solution of PVDF-PVA with BTO nanoparticles: BTO nanoparticles have a diameter of 100 nm. 100 mg of BTO were dispersed in 20 ml of deionized water and sonicated with a 3 mm microtip for 30' with 1sec on/off pulses. Then, 40 mg of dopamine was added to the solution which was placed under magnetic stirring at 60 °C overnight. The BTO solution was centrifuged for 20' at 2200g and re-dispersed in water several times until the desired pH of 6 was obtained. The nanoparticles were vacuum dried at 60 °C overnight. Finally, a certain amount of nanoparticles was mixed with the PVDF-PVA polymer solution and sonicated during 10' before printing. We have labeled this ink as PVDF-PVA-BTO.

Preparation of microcapacitor by inkjet printing: All the microcapacitors were carried out using a *Microdrop technologies* printer with a nozzle size of 70 µm. Printing is controlled by a piezoelectric actuator. The piezo voltage (between 110-120 V) and pulse duration (between 20-26 µs) were adjusted to obtain jetting of single droplets with a volume of ~400 pL before printing the electrode and the dielectric polymers. The temperature of the plate was set at 70 °C to promote fast drying. All inks were filtered (5 µm) before printing. A single line of CNT was printed on the PEN substrate as a bottom and two consecutively lines for top electrodes with a drop spacing of 100 µm.

The surfactant molecules in the electrodes slightly decrease their conductivity. But this effect remains rather limited. As a test, we washed the electrodes by dipping them in a water tank during 24h, and by subsequently drying them at 100°C in vacuum. The conductivity was found to increase by a factor two compared to unwashed electrodes. Considering this limited effect, it was decided to not wash the electrodes because washing makes the process heavier and can alter the dielectric layers. We have observed that the structural integration of the electrode layer remains unchanged when the washing process was performed. PVDF, PVDF-PVA and nanocomposite (PVDF-PVA-BTO) were printed on the bottom electrode with 5 consecutively lines of 20 mm with drop spacings of 50, 75 and 100 µm. After each printed step, the bottom electrode, polymer, and the entire microcapacitor were placed in an oven at 100 °C under vacuum overnight.

Characterization: The dielectric properties of the microcapacitors were recorded as a function of frequency (from 1 to 10^6 Hz) at room temperature using an impedance analyzer (*7260 Impedance Mate Analyzer*). The dielectric breakdown strength and electric displacement−electric field ($P-E$) loops (at 10 Hz) were measured at room temperature in silicone oil by a PolyK ferroelectric polarization loop & dielectric breakdown test system. Prior to all characterizations, each electrode was covered with silver paste and copper wire to

ensure a good contact. The morphology of the electrodes and the dielectric polymer was characterized by scanning electron microscopy (JEOL 6700F).

Supporting Information

Supporting Information is available from the Wiley Online Library or from the author.

Conflict of Interest

The authors declare no conflict of interest.

Acknowledgements

We thank Arkema for providing carbon nanotubes and PVDF materials. The study was partially supported by the Aquitaine Region and the BPI GRAPULE-2 and ANR GAELIC projects. This work has been also partially funded by the CNRS Energy unit (Cellule Energie) through the project MicroPower.

Received: ((will be filled in by the editorial staff))
Revised: ((will be filled in by the editorial staff))
Published online: ((will be filled in by the editorial staff))

References

[1] N. A. Kyeremateng, T. Brousse, D. Pech, *Nat. Nanotechnol.* **2017**, *12*, 7.

[2] D. Qi, Y. Liu, Z. Liu, L. Zhang, X. Chen, *Adv. Mater.* **2017**, *29*, 1.

[3] Z. S. Wu, X. Feng, H. M. Cheng, *Natl. Sci. Rev.* **2014**, *1*, 277.

[4] M. Beidaghi, Y. Gogotsi, *Energy Environ. Sci.* **2014**, *7*, 867.

[5] P. Simon and Y. Gogotsi, *Nat. Mater.* **2008**, *7*, 845.

[6] T. Sharma, S. S. Je, B. Gill, J. X. J. Zhang, *Sensors Actuators, A Phys.* **2012**, *177*, 87.

[7] P. Martins, A. C. Lopes, S. Lanceros-Mendez, *Prog. Polym. Sci.* **2014**, *39*, 683.

[8] R. C. G. Naber, C. Tanase, P. W. M. Blom, G. H. Gelinck, A. W. Marsman, F. J. Touwslager, S. Setayesh, D. M. de Leeuw, *Nat. Mater.* **2005**, *4*, 243.

[9] J. C. Haisheng Xu, Xuerang Fang, Xiaobing Liu, Shan Wu, Yingjun Gu, Xiangjian Meng, Jinglan Sun, *J. Appl. Polym. Sci.* **2011**, *120*, 1510.

[10] I. Bae, S. J. Kang, Y. J. Park, T. Furukawa, C. Park, *Curr. Appl. Phys.* **2010**, *10*, e54.

[11] V. Bhavanasi, V. Kumar, K. Parida, J. Wang, P. S. Lee, *ACS Appl. Mater. Interfaces* **2016**, *8*, 521.

[12] B. M. Aleksander Matavž, *J. Sol-Gel Sci. Technol.* **2018**, *87*, 1.

[13] B. M. Mikolajek, A. Friederich, C. Kohler, M. Rosen, A. Rathjen, J. R. Binder, *Adv. Eng. Mater.* **2015**, *17*, 1294.

[14] V. Matavz, A. Malic, B. and Bobnar, *J. Appl. Phys.* **2017**, *122*.

[15] X. Ding, Y. Li, D. Wang, Q. Yin, *Ceram. Int.* **2004**, *30*, 1885.

[16] J. Jang, H. Kang, H. C. N. Chakravarthula, *Adv. Electron. Mater.* **2015**, *1*, 1.

[17] G. Vescio, R. Leghrib, A. Cornet, A. Cirera, *J. Mater. Chem. C* **2016**, *4*, 1804.

[18] A. Liu, H. Zhu, H. Sun, Y. Xu, Y. Y. Noh, *Adv. Mater.* **2018**, *30*, 1.

[19] X. Zhang, J. Jiang, Z. Shen, Z. Dan, M. Li, Y. Lin, C. W. Nan, L. Chen, Y. Shen, *Adv. Mater.* **2018**, *30*, 1.

[20] B. S. Cook, J. R. Cooper, M. M. Tentzeris, *IEEE Microw. Wirel. Components Lett.* **2013**, *23*, 353.

[21] G. Picci, M. Rabuffi, *IEEE Trans. Plasma Sci* **2002**, *30*, 1939.

[22] Q. M. Chu, B., Zhou, X., Ren, K., Neese, B., Lin, M., Wang, Q., Zhang, *Science (80-.).* **2006**, *313*, 334.

[23] Z. Zhang, T. C. M. Chung, *Macromolecules* **2007**, *40*, 783.

[24] R. I. Haque, R. Vié, M. Germainy, L. Valbin, P. Benaben, X. Boddaert, *Flex. Print. Electron.* **2016**, *1*, 15001.

[25] D. Thuau, K. Kallitsis, F. D. Dos Santos, G. Hadziioannou, *J. Mater. Chem. C* **2017**, *5*, 9963.

[26] C. Allain, L. Limat, *Phys. Rev. Lett.* **1995**, *74*, 2981.

[27] P. Meakin, *Thin Solid Films* **1987**, *151*, 165.

[28] A. T. Skjeltorp, P. Meakin, *Nature* **1988**, *335*, 424.

[29] K. B. Singh, L. R. Bhosale, M. S. Tirumkudulu, *Langmuir* **2009**, *25*, 4284.

[30] J. Zarzycki, M. Prassas, J. Phalippou, *J. Mater. Sci.* **1982**, *17*, 3371.

[31] M. S. Tirumkudulu, W. B. Russel, *Langmuir* **2005**, *21*, 4938.

[32] G. W. Scherer, *J. Am. Ceram. Soc.* **1990**, *73*, 3.

[33] F. Zhang, C. Tuck, R. Hague, Y. He, E. Saleh, Y. Li, C. Sturgess, R. Wildman, *J. Appl. Polym. Sci.* **2016**, *133*, 1.

[34] A. G. Kelly, D. Finn, A. Harvey, T. Hallam, J. N. Coleman, *Appl. Phys. Lett.* **2016**, *109*, 023107.

[35] R. M. E. Goikolea, *Emerging Nanotechnologies In Rechargeable Energy Storage*

Systems, Elsevier, **2017**.

[36] X. Hu, K. Yi, J. Liu, B. Chu, *Energy Technol.* **2018**, *6*, 849.

[37] J. Claude, Y. Lu, Q. Wang, J. Claude, Y. Lu, Q. Wang, *Appl. Phys. Lett.* **2007**, *212904*.

[38] H. Tang, H. A. Sodano, *Nano Lett.* **2013**, 1373.

[39] X. Zhang, B. Li, L. Dong, H. Liu, W. Chen, Y. Shen, C. Nan, *Adv. Mater. Interfaces* **2018**, *5*, 1.

[40] Z. Zhang, Q. Meng, T. C. M. Chung, *Polym.* **2009**, *50*, 707.

[41] Q. Li, K. Han, M. R. Gadinski, G. Zhang, Q. Wang, *Adv. Mater.* **2014**, *26*, 6244.

[42] Q. Chen, Y. Wang, X. Zhou, Q. M. Zhang, S. Zhang, *Appl. Phys. Lett.* **2008**, *92*.

[43] Z. Z. J. Li, X. Hu, G. Gao, Sh. Ding, H. Li, L. Yang, *J. Mater. Chem. C* **2013**, *1*, 1111.

[44] M. X. J. Chen, Y. Wang, H. Li, Huijing Han, X. Liao, R. Sun, X. Huang, *Chem. Mater.* **2018**, *30*, 1102.

[45] F. Guan, J. Wang, L. Yang, J. Tseng, K. Han, Q. Wang, L. Zhu, *Macromolecules* **2011**, *44*, 2190.

[46] J. Wei, Z. Zhang, J. Tseng, I. Treufeld, X. Liu, M. H. Litt, L. Zhu, *ACS Appl. Mater. Interfaces* **2015**, *7*, 5248.

[47] Y. Qiao, M. S. Islam, K. Han, E. Leonhardt, J. Zhang, Q. Wang, H. J. Ploehn, C. Tang, *Adv. Funct. Mater.* **2013**, *23*, 5638.

[48] A. F. Baldwin, R. Ma, A. Mannodi-kanakkithodi, T. D. Huan, C. Wang, M. Tefferi, J. E. Marszalek, M. Cakmak, Y. Cao, R. Ramprasad, G. A. Sotzing, *Adv. Mater.* **2015**, *27*, 346.

[49] Q. M. Z. Y. Wang, X. Zhou, M. Lin, *Appl. Phys. Lett.* **2015**, *96*, 202905.

[50] Z. X. W. Li, Q. Meng, Y. Zheng, Zh. Zhang, W. Xia, *Appl. Phys. Lett.* **2013**, *96*, 192905.

[51] D. M. Joyce, N. Venkat, F. Ouchen, K. M. Singh, S. R. Smith, A. Christopher, P. T. Murray, J. G. Grote, D. M. Joyce, N. Venkat, F. Ouchen, K. M. Singh, S. R. Smith, C. A. Grabowski, P. T. Murray, J. G. Grote, *J. Appl. Phys.* **2014**, *115*, 114108.

[52] F. Guan, J. Pan, J. Wang, Q. Wang, L. Zhu, *Macromolecules* **2010**, *43*, 384.

[53] Y. Chen, X. Tang, J. Shu, X. Wang, W. Hu, Q. Shen, *J. Polym. Sci.* **2016**, *54*, 1160.

[54] M. Zhang, L. Zhang, M. Zhu, Y. Wang, N. Li, Z. Zhang, Q. Chen, L. An, Y. Lin, C. Nan, *J. Mater. Chem. A* **2016**, *4*, 4797.

[55] V. Tomer, E. Manias, C. A. Randall, *J. Appl. Phys.* **2011**, *110*.

[56] M. Roy, J. K. Nelson, R. K. MacCrone, L. S. Schadler, C. W. Reed, R. Keefe, W. Zenger, *IEEE Trans. Dielectr. Electr. Insul.* **2005**, *12*, 629.

Figures:

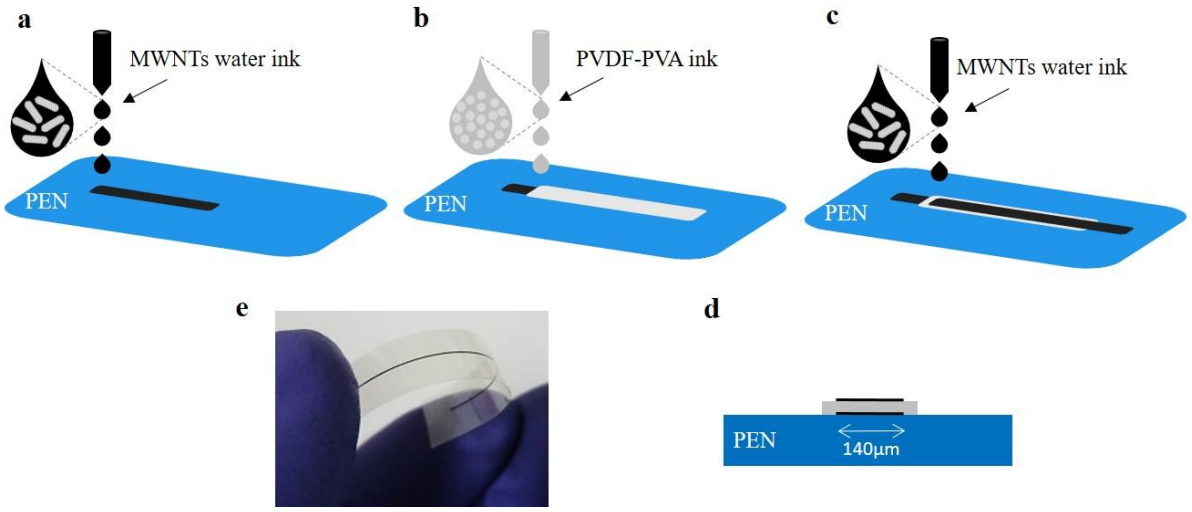

Figure 1. Schematic representation of the fabrication process of microcapacitor with inkjet printing technique. **a,** Bottom electrode printed on PEN substrate using CNT water ink. **b**, PVDF-PVA ink printed on the top of the bottom electrode, serving as dielectric polymer layer. **c,** Printing top CNT electrode on top of the dielectric polymer layer, which does not contact with the bottom electrode. **d,** Lateral view of the designed microcapacitor with an effective electrode width of around 140 μm. **e,** Photograph of bended flexible microcapacitor with an effective area of ~2.8×10^{-6} m^2.

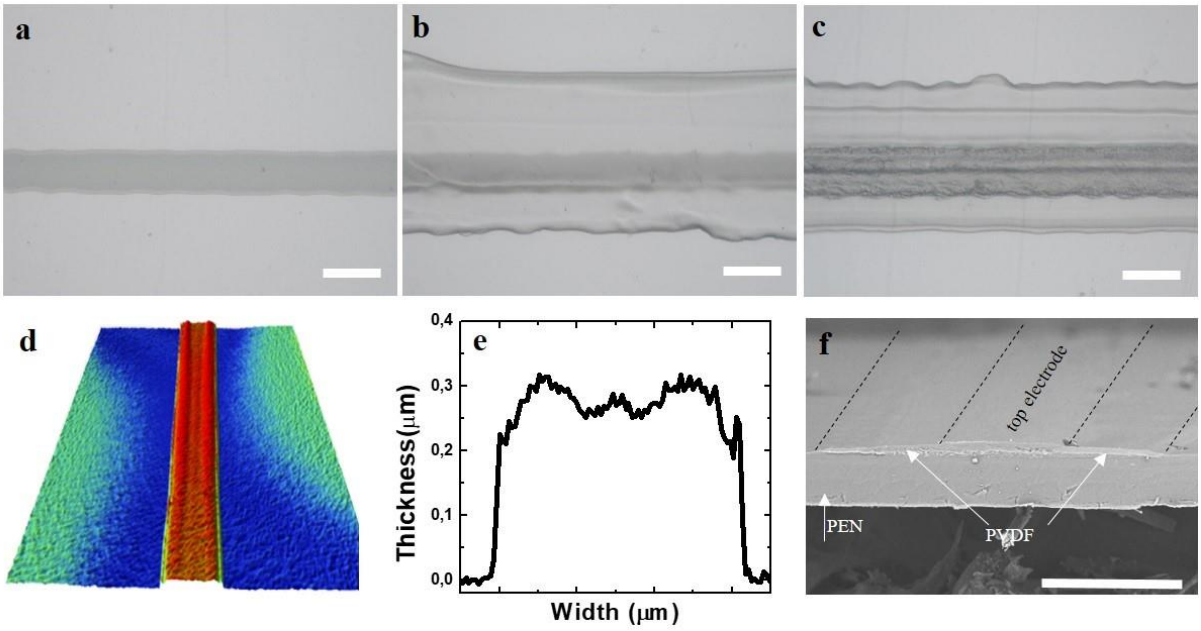

Figure 2. **a**, Microscopic image of the printed bottom CNT electrode. **b**, Optical micrograph of the printed PVDF-PVA layer on the bottom CNT electrode. **c**, Microscopic image of the sandwiched structure with two CNT electrodes and PVDF-PVA layer in between. **d**, 3D image of the thickness profile for the bottom CNT electrode. **e**, A typical thickness profile of the bottom electrode. **f**, SEM image of the sectional view of the printed microcapacitor on PEN substrate. Scale bar 200 μm.

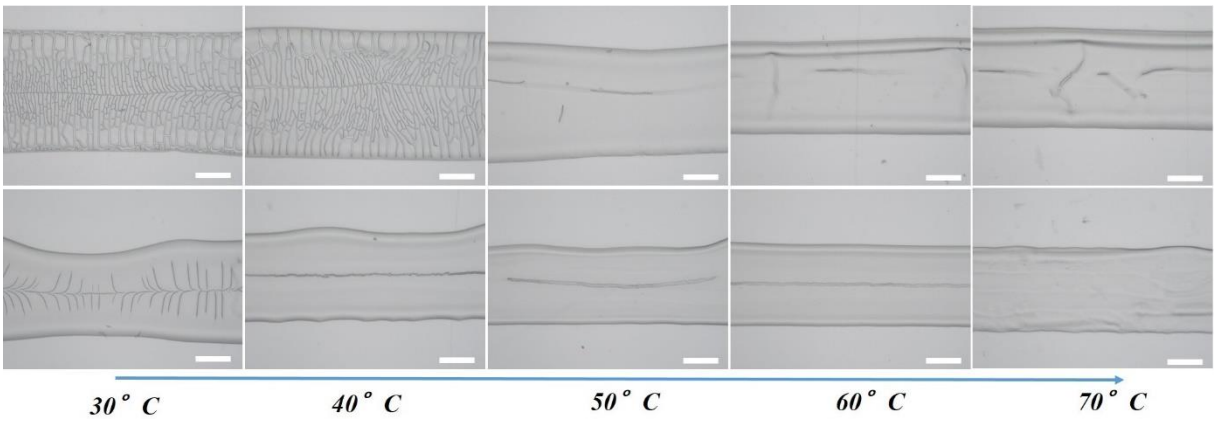

Figure 3. Microscopic images of dielectric layers printed with pure PVDF latex (upper) and PVDF-PVA mixture ink (bottom) on PEN substrate at different temperatures. Scale bar 200 μm.

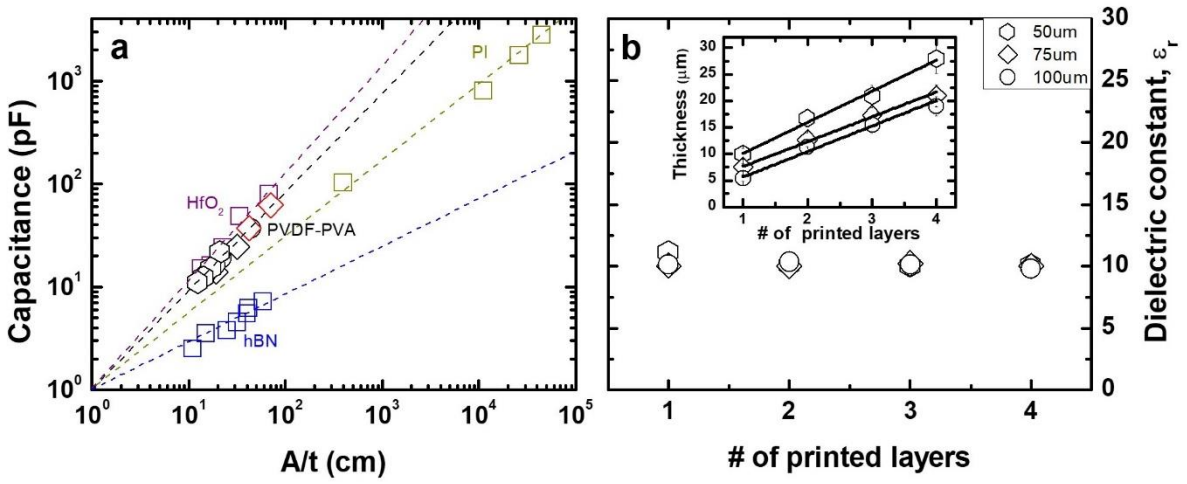

Figure 4. **Tailored capacitive behavior of the printed microcapacitors**. **a,** Dependence of the capacitance on the area/thickness (A/t) ratio for our printed microcapacitor printed capacitors based on polymers and ceramics in the literature.[17,33,34] **b**, The dielectric constant is observed to remain nearly constant over the whole range of printing layer numbers and drop spacing. Inset in **b** shows the polymer layer thickness as a function of the printing layer number for different drop spacings.

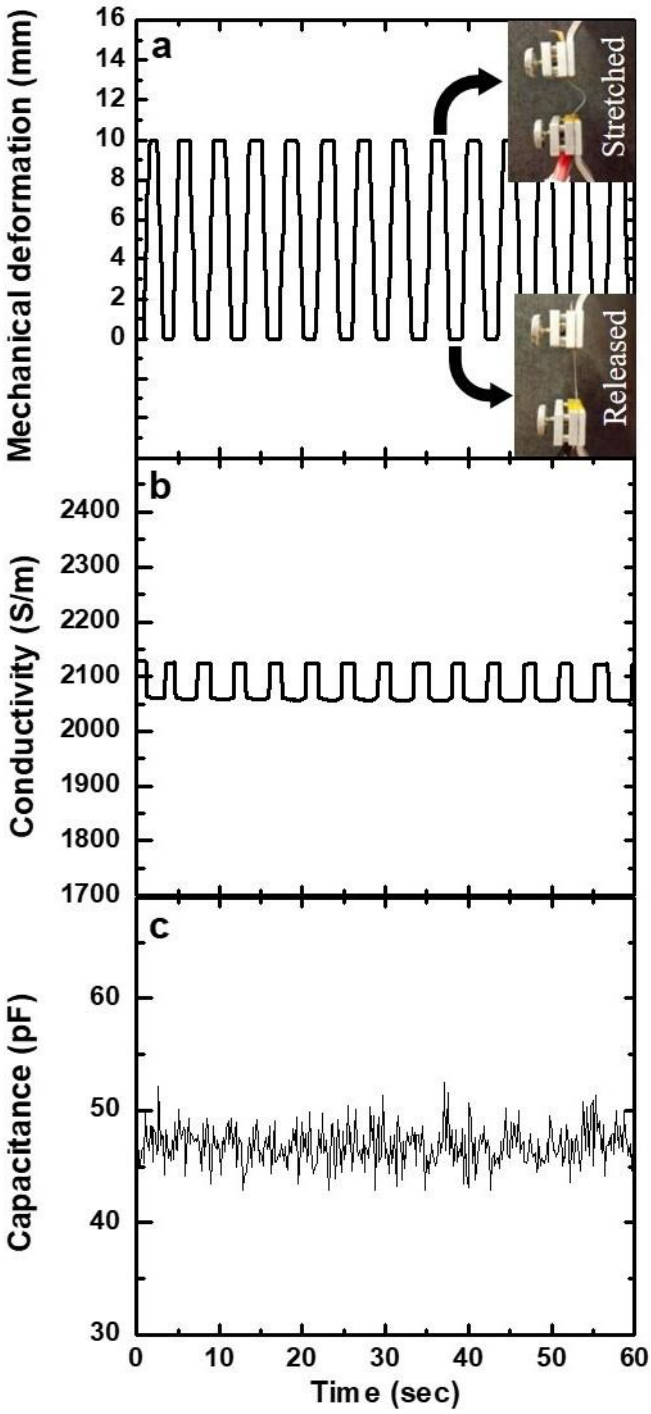

Figure 5. a, Mechanical bending deformation was applied on the printed materials to study their performance stability. **b**, Variation of conductivity of printed CNT electrode with time. **c**, Variation of capacitance of the printed microcapacitor as a function of time. Negligible conductivity variation can be observed for the electrode, resulting from the good adhesion of the nanotubes to the PEN substrate.

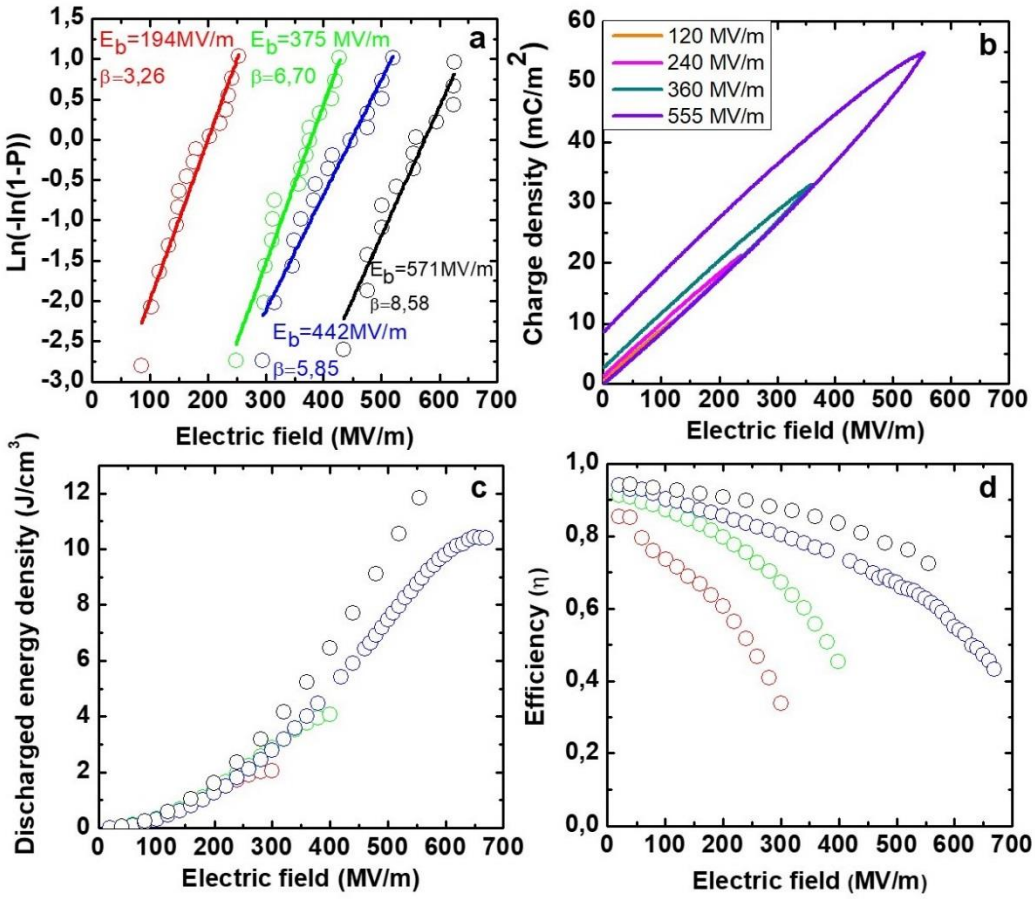

Figure 6. **Energy storage properties of printed microcapacitors**. **a**, Cumulative failure probability distribution of printed PVDF-PVA film with different layer numbers as a function of electric field. **b**, *P*–*E* loops of microcapacitors printed with d_s=75 μm and four printing layers under different electric fields. **c**, Calculated discharged energy density from the *P*–*E* loops of printed microcapacitors with different layers as a function of electric field. **d**, Variation of charge–discharge efficiency with electric field for printed microcapacitors with different PVDF-PVA layers. **a-d**, 1 PVDF-PVA layer (Red), 2 layers (Green), 3 layers (Blue) and 4 layers (black).

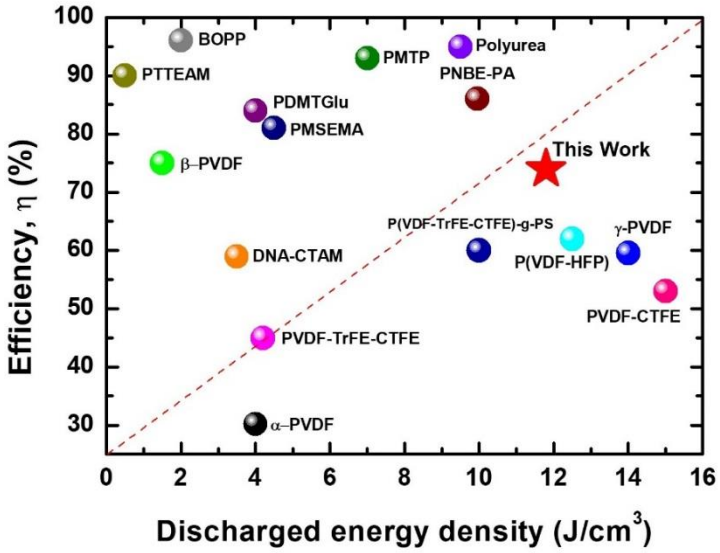

Figure 7. Efficiency vs. discharged energy density near its breakdown strength of microcapacitor printed with 4 layers, which is compared to others dielectric polymers reported in previous studies.[43,44,53,54,45–52] All references values correspond to a dielectric capacitor prepared by conventional techniques except inkjet printing.

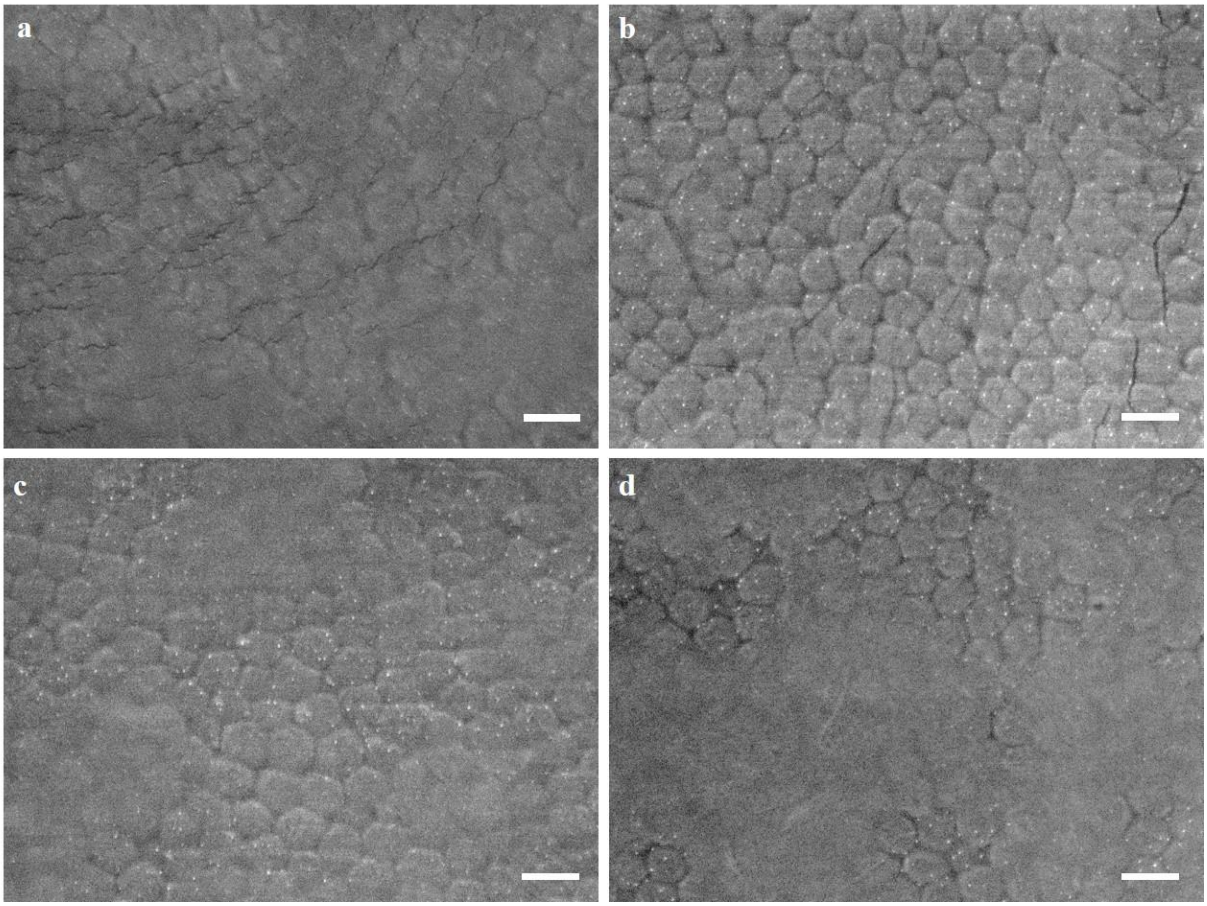

Figure 8. SEM pictures of the surface morphologies of printed PVDF-PVA layers with different number of layers: **a**, 1, **b**, 2, **c**, 3 and **d**, 4 printed layers of PVDF-PVA. Scale bar 200 nm. 1 and 2 printed layers show cracks in the film preventing to exploit the maximum discharged energy density. On the other hand, no cracks presented in film with 3 and 4 printed layers, giving a discharged energy density of more than 10 Jcm^{-3}.

ToC:

Fernando Torres-Canas and coworkers demonstrate a flexible and fully inkjet-printed high-energy microcapacitor based on aqueous dielectric inks composed of PVDF latex and PVA binders. This approach uniquely combines the high breakdown strength of PVA and high polarization of PVDF, making the printed microcapacitors promising for demanding printed electronics that require micro-scale peak powers.

Keyword: Flexible electronics

Fernando Torres-Canas, Jinkai Yuan*, Isabelle Ly, Wilfrid Neri, Annie Colin, and Philippe Poulin*

Title
Inkjet Printing of Latex Based High-Energy Microcapacitors

ToC figure

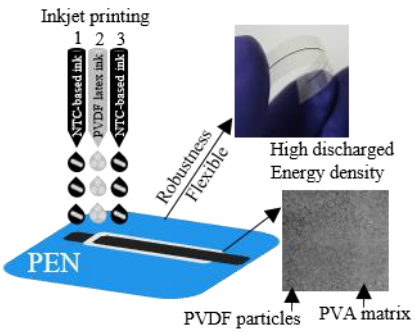

WILEY-VCH

Supporting Information

Inkjet Printing of Latex Based High-Energy Microcapacitors

Fernando Torres-Canas, Jinkai Yuan, Isabelle Ly, Wilfrid Neri, Annie Colin, and Philippe Poulin**

Univ. Bordeaux, CNRS, Centre de Recherche Paul Pascal, UMR5031, 33600 Pessac, France
E-mails: jinkai.yuan@crpp.cnrs.fr, philippe.poulin@ crpp.cnrs.fr

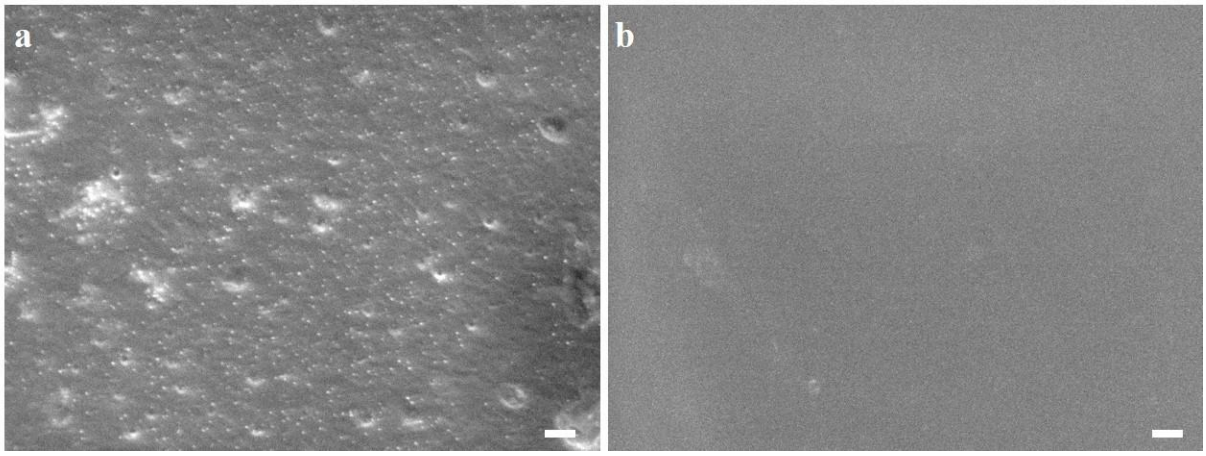

Figure S1. SEM pictures of the surface of films based on **a)** pure PVDF latex and **b)** pure PVA, which are prepared by spin coating. Scale bar 200 nm. Voids are observed for the PVDF film but a homogeneous film is obtained for PVA.

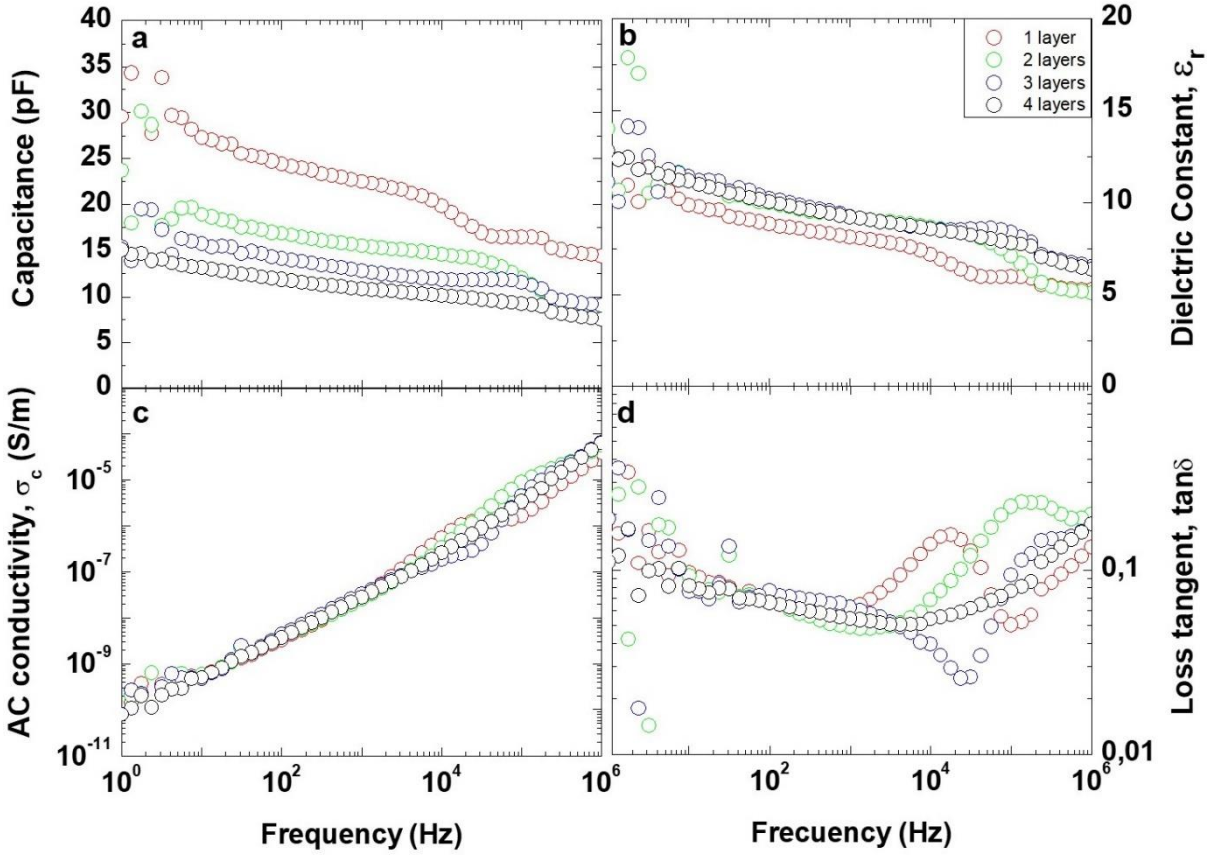

Figure S2. Frequency dependence of **a)** capacitance, **b)** dielectric constant, **c)** AC conductivity and **d)** loss tangent of microcapacitors based on PVDF-PVA layers which are printed with a drop spacing of 75 µm. Capacitance decreases as a function of the number of printed layers. The dielectric constant remains nearly constant (~10) at 100 Hz. AC conductivity shows a typical behavior of dielectric material, and the loss tangent is around 0.06 at 100 Hz.

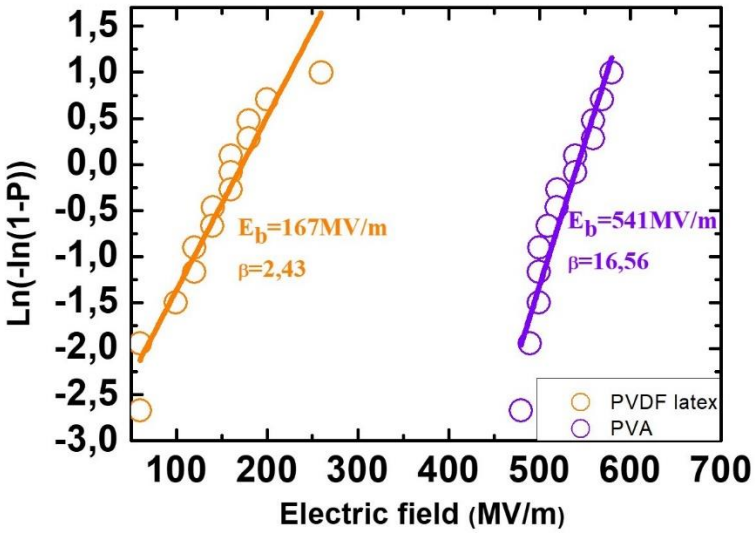

Figure S3. Weibull distribution of breakdown strength for pure PVA and PVDF latex films prepared by spin coating.

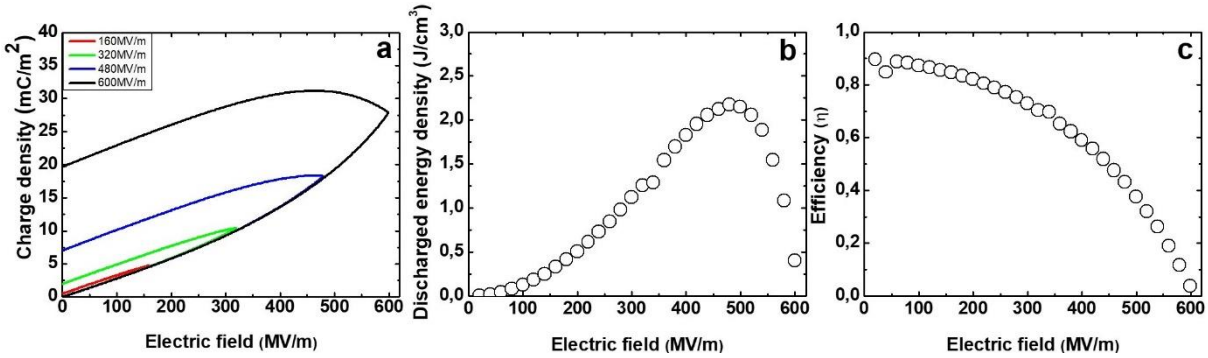

Figure S4. **a)** *P-E* loops, **b)** discharged energy density and **c)** efficiency for a PVA film prepared by spin coating. Low discharged energy density is achieved even at high electric fields.

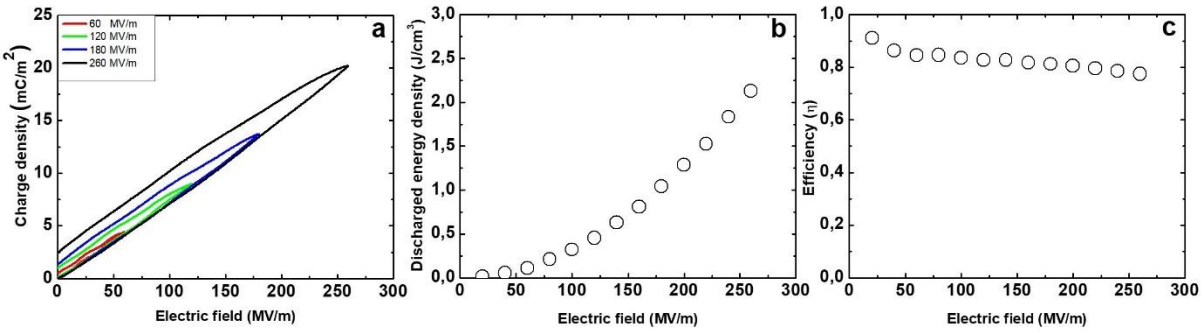

Figure S5. **a)** *P-E* loops, **b)** discharged energy density and **c)** efficiency for a pure PVDF latex film prepared by spin coating. The maximum discharged energy density is around ~2 Jcm^{-3}. This low value is likely due to the presence of voids and cracks in the film.

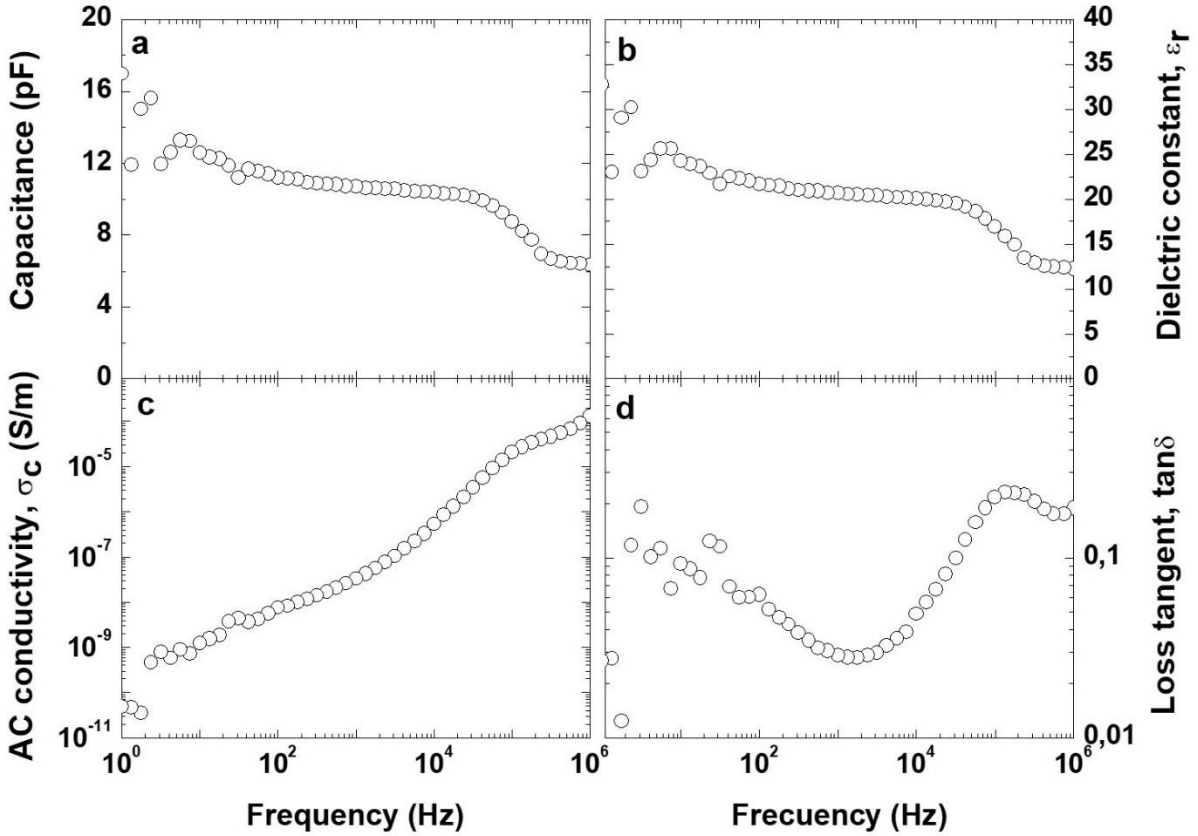

Figure S6. Frequency dependence of the: **a)** capacitance, **b)** dielectric constant, **c)** AC conductivity and **d)** loss tangent for a printed PVDF-PVA-BTO nanocomposite . Higher values of capacitance and dielectric constant are obtained, while the loss tangent still remains low (~0.06). 8 layers of PVDF-PVA-BTO materials give a capacitance of around 12 pF for a thickness of around 48µm. The incorporation of BTO nanoparticles allows for obtaining a maximum dielectric constant of ~20, almost twice than that of PVDF-PVA. The low AC conductivity found here is typical for a polymer composite made of insulating materials. The dielectric losses can compare with the losses of the PVDF-PVA systems.

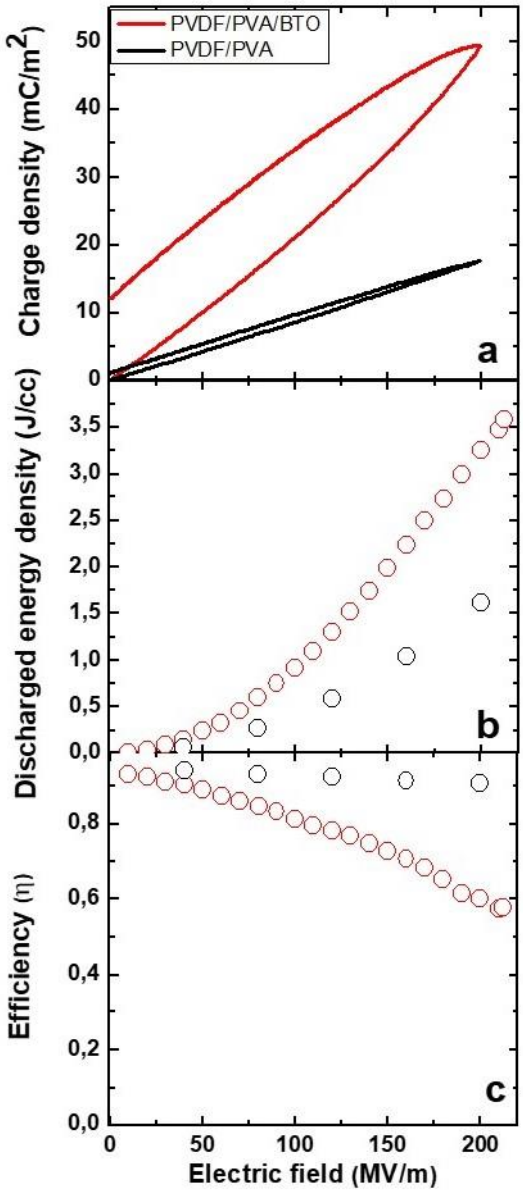

Figure S7. **a)** *P-E* loops, **b)** discharged energy density and **c)** efficiency of PVDF-PVA layers and PVDF-PVA-BTO nanocomposite layers. At low electric field the discharged energy density is almost twice the energy density of the PVDF-PVA. However, the efficiency is lower. At 200 MVm^{-1} the nanocomposite PVDF-PVA-BTO has a maximum charge density of ~50 mCm^{-2} which is 2.7 times higher than the system PVDF-PVA (~18 mCm^{-2}). Regarding the discharged energy density, a value of ~3.5 Jcm^{-3} at 200 MVm^{-1} is found for the PVDF-PVA-BTO nanocomposite, which shows an improvement of 233% as compared to the PVDF-PVA. Such enhancement is due to the high dielectric constant of the nanocomposite. In terms of efficiency, the nanocomposites have a value of 0.7, which is lower as compared to PVDF-PVA systems.